Asian Journal of Chemistry; Vol. 33, No. 6 (2021), 1253-1260

ASIAN JOURNAL OF CHEMISTRY

https://doi.org/10.14233/ajchem.2021.23169

Enhancing the Performance and Recyclability of Polyaniline/TiO_2 Hybrid Nanocomposite by Immobilizing with Zein/Hydroxyethyl Cellulose Composites for Removal of Anionic Dyes

TADESSE BASSIE GELAW and BALLADKA KUNHANA SAROJINI*

Department of Industrial Chemistry, Mangalore University, Mangalagangothri-574199, India

*Corresponding author: E-mail: bksaroj35@gmail.com; tadesse.bassie892@gmail.com

Received: 16 February 2021; *Accepted*: 23 March 2021; *Published online*: 5 June 2021; AJC-20352

Fabrication of a stable, recyclable and eco-friendly photocatalyst for dye treatment is vital in sustaining a clean ecosystem. In this regard, polyaniline/TiO_2 (PANI/TiO_2) photocatalyst was immobilized by zein/hydroxyethyl cellulose (zein/HEC) adhesive to enhance recyclability and catalytic activity. The blending of zein/HEC/PANI/TiO_2 photocatalyst involves *in situ* oxidative polymerization, followed by immobilization with zein/HEC functionalized composites. The PANI/TiO_2 composite was successfully grafted with the adhesive through physicochemical interaction, as evidenced by field emission scanning electron microscope (FESEM), Fourier transform infrared spectroscopy (FTIR) and powder X-ray diffractometer (XRD). The simultaneous thermal analysis (STA) results show that the photocatalyst has the best thermal stability relative to PANI and PANI/TiO_2 in the recommended range of dye degradation temperature. The effect of external factors like TiO_2 nanoparticle proportion, pH of the solution and catalyst dosage was studied in response to dye degradation capacity. The synthesized catalyst is efficient to degrade methyl orange in a wide range of pH. The kinetics of the catalysis reaction obeys the first order kinetics. The maximum degradation efficiency achieved was 97.9% and 84.3% in the presence and absence of light, respectively. The catalyst was easily recovered by decantation and its catalytic efficacy was more than 94% after 5 cycles. Hence, it is a promising alternative for decolourizing anionic dyes from wastewater.

Keywords: Zein/HEC, PANI/TiO_2, Photocatalyst, Recyclability, TiO_2 nanoparticle, Hydroxyethyl cellulose.

INTRODUCTION

The worldwide development of industries contributes to an increase in the release of different hazardous wastes to the environment. Among the harmful wastes, dyes are the primary toxic and persistent organic chemicals released from textile, pharmaceutical, food, paper and cosmetic industries. From the overall quantity of dyes produced globally, over 10% are released to the water body as wastes [1]. This reduces dissolved oxygen levels [2] and photosynthesis rate in the aquatic system [3]. In addition, they are also poisonous and carcinogenic agents to living organisms [4]. Different approaches like adsorption [5], coagulation [6], filtration [7], ozonation [8], biodegradation [9], photocatalytic degradation [10], have been developed to address these problems. Most of these methods have drawbacks, such as low-performance capacity, producing secondary pollutants, low stability, require huge investment and complex separation processes [11]. Many studies showed that photocatalytic degradation had become the most preferred choice for the removal of dyes. Since, it is economical [12] and the final degradation products have no negative impact on the ecosystem [13]. Thus, it is essential to develop a recyclable, efficient and stable photocatalyst to remove wastewater dyes.

In the present study, TiO_2 nanoparticle is selected for the photocatalytic agent due to its chemical stability, non-toxicity, compatibility and conductivity [14]. However, it was reported that the agglomeration of nanoparticles and recombination of excited electrons due to strong coulombic interaction strongly affect its catalytic activity during the reaction [15,16]. Hybridizing it with conductive polymers can reduce the instability of charge separation between the valence and conduction band and agglomeration of nanoparticles [17]. Polyaniline is the one that was exclusively used to boost the photocatalytic function of TiO_2. Because it possesses lower bandgap energy and can easily excite electrons by absorbing light. Thus, TiO_2 nanoparticles in the hybrid composite trapped excited electrons from

polyaniline to its conduction band and hence the catalytic reaction is enhanced due to electron-hole stabilization [18]. In addition, polyaniline is commonly used for these purposes due to its biocompatibility, high electrical conductivity, chemical stability and ease of synthesis [19]. However, it is not easy to recover the slurry of polyaniline/TiO_2 from the final product, particularly in large scale treatment [20,21]. Furthermore, these suspensions from the reaction medium prevent the incoming light from penetrating the entire part of the reaction system [22]. This effect limits the performance capacity of the photocatalyst in addition to the challenge of separation. Accordingly, it is essential to enhance the photocatalytic efficiency and recyclability of polyaniline/TiO_2 (PANI/TiO_2) photocatalyst. Thus, this study deals with improving and immobilizing PANI/TiO_2 photocatalyst by zein/hydroxyethyl cellulose (zein/HEC) functionalized composites.

Zein is composed of prolamine protein containing more than 50% hydrophobic residues of amino acids. Its hydrophilic nature can be enhanced by blending with water-soluble polymers due to hydrogen bonding between constituent species [23]. Composites of zein with hydrophilic polymer also possess a rough structure with high surface area microholes due to the self-aggregation of hydrophobic amide groups favoured by hydrophilic group repulsion [24]. Besides, many active groups disclosed and positively charged functionalized networked porous structure of zein formed in acidic condition [25,26]. The microholes, functionalized porous structures and different functional groups produce synergetic properties towards absorption [23,27]. This property is essential to support the adsorption of dye pollutants to the heterogeneous catalyst surface. Furthermore, the strong interaction between zein and polyaniline makes the photocatalyst immobilization effective [28].

Hydroxyethyl cellulose is a well-known non-ionic stabilizer, binder and water retainer in various composite products due to its high viscosity and stability in all pH ranges [29,30]. Hence, the composite of zein and hydroxyethyl cellulose is therefore suggested to be a stable and absorbing composite. Based on these facts, blending PANI/TiO_2 with zein/HEC composite immobilizes and increases adsorptive-assisted catalytic function due to the combined effects of factionalized structures and various active groups.

In past, materials like polyacrylonitrile [31], polystyrene cubes [32], poly(vinyl alcohol) [33], diazonium salt [34], polyvinyl chloride (PVC) and epoxidized natural rubber (ENR-50) [35], *etc.* were used to immobilize and increase the recyclability of polyaniline/TiO_2 composite. But some of the immobilizers lower the efficiency of the catalyst [32] and others are toxic, such as polyvinyl chloride and epoxides [36]. Thus, it is reasonable to immobilize PANI/TiO_2 photocatalyst with non-toxic adhesive materials without affecting its catalytic activity. In this regard, glutaraldehyde crosslinked zein/HEC composite was used for anchoring PANI/TiO_2 and enhancing the photocatalytic activity. So far, there was no report on polyaniline/TiO_2 photocatalyst immobilized by zein/HEC composite polymer. Therefore, the objective of this work was to study the combined effect of zein and hydroxyethyl cellulose composite on PANI/TiO_2 adsorptive assisted photocatalytic property for the degradation of anionic dye wastes. The newly synthesized zein/HEC/PANI/TiO_2 photocatalyst was characterized by FESEM connected with energy dispersive X-ray (EDX), thermal, XRD and FTIR techniques. The TiO_2 nanoparticles proportion, catalyst dosage and pH on the photocatalytic degradation reaction were optimized. The kinetics of the reaction was also evaluated using first order kinetic models. Furthermore, the photocatalyst's feasibility study was assessed by recycling and comparing it with previous reports.

EXPERIMENTAL

Aniline with purity 99% was procured from Spectrochem (Mumbai, India). α-Zein (Analytical reagent) and a mixture of 20% rutile and 80% of anatase TiO_2 (<100 nm size) were obtained from Sigma-Aldrich (USA). Ammonium persulphate (purity, 98%) was purchased from Sisco research laboratory Pvt. Ltd. (India) and HCl (purity, 35-37%) was obtained from Alpha Chemika (India). Glutaraldehyde (purity, 25%) and high viscosity HEC (viscosity, 250-450 mPas at 2% H_2O & 20 ºC) were purchased from LOBA Chemie, India.

Synthesis of zein/HEC/PANI/TiO_2 composite: PANI/TiO_2 hybrid nanocomposites were fabricated by oxidative *in situ* polymerization. An equimolar concentrations of ammonium persulphate and aniline were prepared using 1 M HCl. Both solutions were stirred in a separate container until a clear, transparent solution was formed. Presonicated aqueous solution of TiO_2 nanoparticles was added to the polyaniline solution and stirred for 0.5 h. This solution temperature was adjusted to 0-5 ºC in an ice bath. With continuous stirring, ammonium persulphate solution was added and stirring continued for 5 h. This green acidic solution pH was adjusted to three to prevent zein breakdown during mixing [37].

Zein functionalization was performed by dissolving zein powder in dilute HCl using the previous standard method with a slight modification [25]. Typically, HCl (0.4 M) was prepared in 70% ethanol solution. Then zein powder was transferred to this solution. The reaction mixture was stirred for 12 h at 70 ºC to convert hydrophobic amine groups of zein to hydrophilic ones. Hydroxyethyl cellulose solutions were also dissolved separately in 50% ethanol solution. The hydroxyethyl cellulose and zein solution were mixed with a glutaraldehyde crosslinker and stirred overnight. The green polyaniline/TiO_2 composite solution was added to the zein/HEC gel solution and stirred for 12 h to immobilize photocatalyst. Then it was neutralized by adding NaOH until the pH becomes above six and precipitated by adding excess water. It was allowed to settle all the precipitates. After decanting the supernatant, it was washed with water, followed by acetone. Zein/HEC/PANI/TiO_2 composite obtained was transferred to an oven set at 60 ºC for drying in 12 h. Finally, it was crushed into small size. In the same procedure, the hybrid composites with different proportions of TiO_2 were prepared for further characterization.

Characterization: The elemental composition and morphology of the hybrid composite were determined by FESEM connected with the EDX analyzer (CARL ZE155, OXFORD instruments EDX, USA). The possible interactions and functional groups present in the composite were confirmed by FTIR

(IRPrestige-20, Shimadzu, Japan) in the wave ranging from 2000 to 400 cm^{-1}. XRD (PANALYTICAL, X'PERT PRO, CuKα radiation) was used to determine composite (crystal structure or amorphous) patterns. The thermal stability of the hybrid nanocomposite was performed using STA 6000, Perkin-Elmer, USA with a heating rate of 10 ºC per min at a temperature range of 25 to 800 ºC under normal conditions.

Adsorptive assisted photocatalytic study: The adsorptive assisted photocatalytic study was performed using batch photoreactors. In this experiment, 0.03 g of the photocatalyst was immersed in a catalytic bath containing 100 mL of 125 µM of methyl orange and stirred continuously. After 30 min of adsorption in the dark environment, it was irradiated with an 18 W UV light source with a wavelength of 395 nm. In a predetermined interval, 4 mL of sample was withdrawn and the analyte concentration was determined by UV-Vis spectrophotometer (UV-1800, Shimadzu, Japan). For recycling, zein/HEC/PANI/TiO_2 composite was allowed to settle for 0.5 h and then isolated from the first phase by decantation. After that, it was washed with acidic water followed by distilled water repeatedly and rinsed with acetone. Finally, it was dried in an oven set at 60 ºC before using for the second cycle with a freshly prepared methyl orange solution. A similar procedure was used for the rest of the cycles. The catalytic efficiency (η) of hybrid composite was calculated from eqn. 1:

$$\eta = \frac{C_o - C_e}{C_o} \times 100 \quad (1)$$

where C_o and C_e are the initial and equilibrium dye concentrations of the solution respectively.

RESULTS AND DISCUSSION

Morphology: Zein/HEC/PANI/TiO_2 composite morphology was described in comparison with pure polyaniline and PANI/TiO_2 composite as shown in Fig. 1. Most of the polyaniline molecules had long road-like fibers (Fig. 1a). The addition of TiO_2 nanoparticles changed this structure and formed short length fibers (Fig. 1b). This shows that TiO_2 nanoparticles interacted with polyaniline molecules and preventing long chain road-like structure formation. In Fig. 1c, a porous crosslinked networked structure with some fibers was also observed indicated that PANI/TiO_2 was partially grafted in the polymer matrix of zein/HEC composite network. The average particle size was computed by counting more than 150 particles from the FESEM image using Image J software. Based on this calculation, the average dimensions of polyaniline, PANI/TiO_2 and Zein/HEC/PANI/TiO_2 nanoparticles were 53.21, 46.13 and 61.64 nm, respectively. In addition to morphological changes, it is also essential to describe major constituent species present in the composite using EDX. The elements, O, C, N and Ti were expected components in the composite. From the EDX spectrum (Fig. 1a), there were no spectral peaks related to Ti, while Ti peaks were observed in Fig. 1b-c confirmed that TiO_2 nanoparticles were involved in the hybrid composite. Both the weight and atomic percent of nitrogen were also negative in pure polyaniline and PANI/TiO_2 composite, confirmed that nitrogen content was less and could not be detectable. However, as shown in Fig. 1c of EDX graph, nitrogen appeared due to zein/HEC composite addition. This was the indication for nitrogen containing groups (zein) in the composite [28]. The percen-

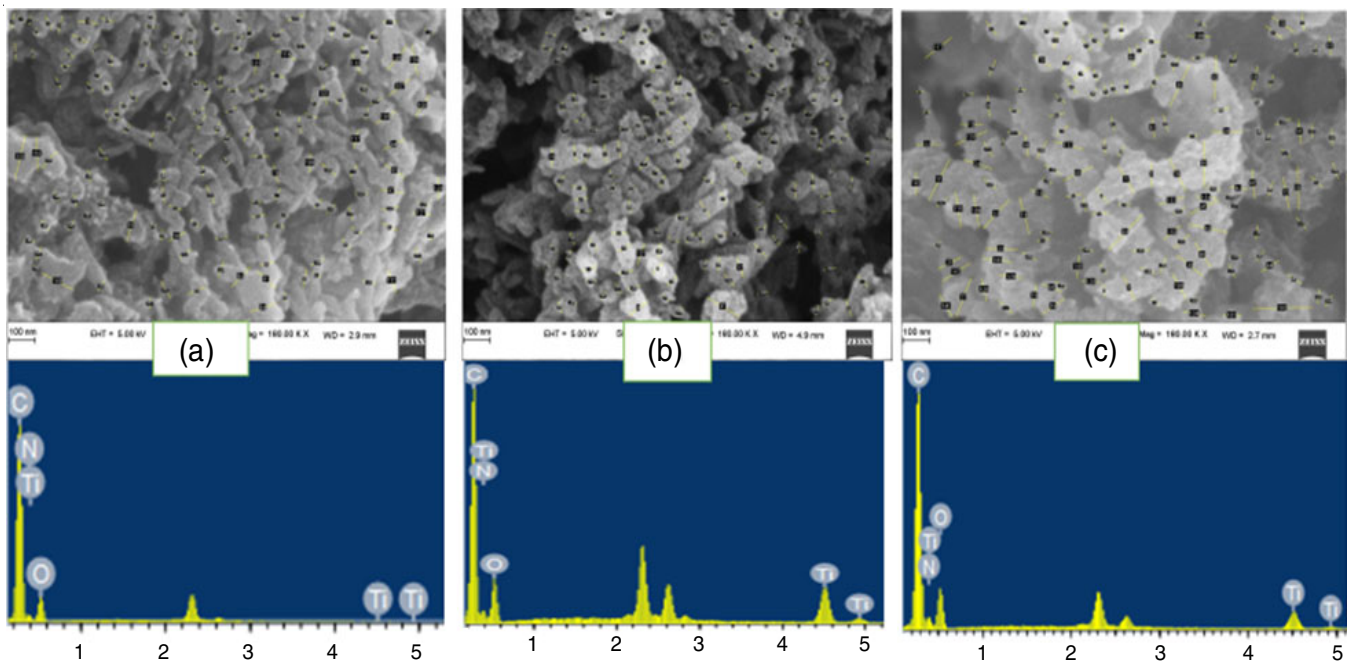

Element	Weight%	Atomic%	Compd.%	Formula
N K	-0.22	-7.70	0.00	
O K	2.57	71.33	3.54	O2C
Ti K	0.01	0.11	0.00	
C	0.97	35.66		
Total	3.32			

Element	Weight%	Atomic%	Compd.%	Formula
N K	-0.22	-4.27	0.00	
O K	3.65	62.31	5.05	O2C
Ti K	1.89	10.80	0.00	
C	1.37	31.16		
Total	6.69			

Element	Weight%	Atomic%	Compd.%
N K	0.05	0.92	0.00
O K	3.76	61.55	5.17
Ti K	1.23	6.75	0.00
C	1.41	30.78	
Total	6.45		

Fig. 1. FESEM-EDX graphs of (a) PANI, (b) PANI/TiO_2 and (c) zein/HEC/PANI/TiO_2

tage composition of components in polyaniline and PANI/TiO_2 changed with the addition of TiO_2 nanoparticle and zein/HEC composite, respectively (Fig. 1b-c). This also confirmed that TiO_2 nanoparticles and zein/HEC composites took part in the hybrid composite formation.

X-ray diffraction (XRD) studies: The XRD patterns of glutaraldehyde crosslinked zein/HEC composite, pure PANI, PANI/TiO_2 and zein/HEC/PANI/TiO_2 were compared. Hydroxyethyl cellulose has no XRD diffraction peaks [38]. Hence, the two broad peaks as observed in Fig. 2a were due to zein, indicated that the composite was structurally amorphous [39]. In Fig. 2b, the peaks at 2θ = 8.9º and 14.96º were the distinct doping diffraction of low crystalline polyaniline. The peaks at 2θ = 21.04º and 25.34º confirmed the presence of polyaniline emeraldine chain with repeated units [40-42]. The peaks observed in Fig. 2c at 2θ = 25.35º, 37.85º, 48.04º, 54.13º, 55.13º and 62.87º were due to anatase TiO_2 nanoparticles in the hybrid nanocomposite [14,18,43]. In Fig. 2c-d, there were similar peaks of TiO_2 nanoparticle with a slight variation in intensity, indicating that the crystal structure of TiO_2 present in the hybrid nanocomposite was not affected by either the polyaniline or the zein/HEC composite, similar with the previous report [43]. The average crystal size was estimated from the Debye-Scherrer's equation:

$$d_{DRX} = \frac{k\lambda}{b\cos\theta} \quad (2)$$

where d is the diameter of the crystal, λ is the wave length of X-ray radiation, k is a constant = 0.15418, B is the line width at the half maximum intensity and θ is the Bragg diffraction angle. The proximate average crystal size calculated from eqn. 2 were 4.86, 11.73 and 11.36 nm for PANI, PANI/TiO_2 and zein/HEC/PANI/TiO_2, respectively. The proximate average crystal size between PANI/TiO_2 and zein/HEC/PANI/TiO_2 also confirmed that TiO_2 nanoparticle was not affected by the composite material.

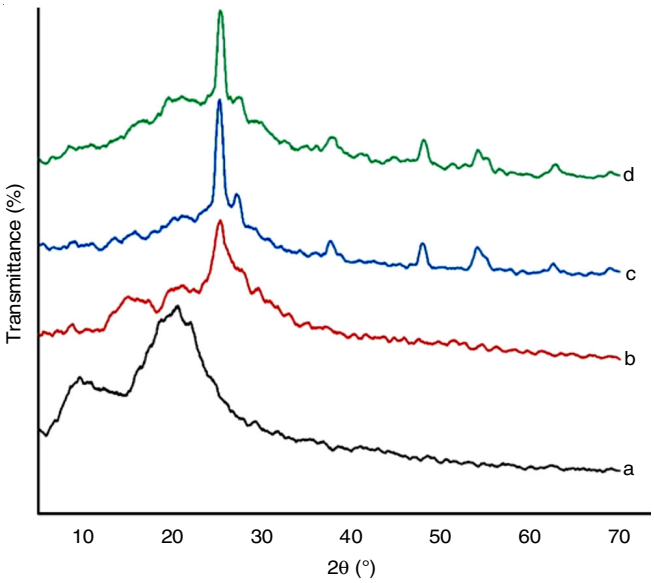

Fig. 2. XRD peaks of (a) zein/HEC, (b) Pure PANI, (c) PANI/TiO_2 and (d) zein/HEC/PANI/TiO_2 hybrid nanocomposites

FTIR studies: The characteristics FTIR peaks of PANI, PANI/TIO_2, zein/HEC/PANI/TiO_2 and glutaraldehyde crosslinked zein/HEC/PANI/TiO_2 are shown in Fig. 3. The quinoid (C=N) and benzoid (C=C) unit ring stretching vibrations were observed in the wavenumber of 1557 and 1462 cm^{-1}, respectively as shown in Fig. 3a [44]. These two units confirmed the formation of emeraldine polyaniline. The peak corresponding to C-N stretching in the benzenoid unit was observed at the wavenumber of 1285 cm^{-1} [45]. At 1230 cm^{-1}, protonated conductive polyaniline emeraldine salt characteristic was also observed due to C-N^+ stretching vibration [46]. The peaks around 791 and 1020 cm^{-1} were due to out plane and in-plane bending vibrations of =C-H, respectively [47]. In Fig. 3b, the features polyaniline peaks of C=C and C-N (1462 and 1285 cm^{-1}) were observed at higher wave numbers (1472 and 1291 cm^{-1}) due to Ti-N interaction in the composite [48], while the peak corresponding to quinone remains unchanged. All the characteristics peaks of pristine polyaniline observed between 2000 and 450 cm^{-1} were also present in PANI/TiO_2 composite and new peaks appeared at 572 and 501 cm^{-1} due to TiO_2 nanoparticles as shown in Fig. 3b [49]. But some peaks shifted to higher wavenumbers and decrease in intensity in PANI/TiO_2 composite due to the surface interactions of TiO_2 nanoparticles with hydrogen bonds and N-H groups in polyaniline [50]. In Fig. 3c, almost all the peaks appeared in polyaniline and PANI/TiO_2 were also observed with additional spectrum in 1652 cm^{-1} due to amide-I. More peaks around 1557 and 1285 cm^{-1} due to amide II and III were also expected but overlapped with the peaks of quinone and benzene ring stretching vibrations, respectively. The strong and sharp spectral peaks observed in Fig. 3c became diminished as shown in Fig. 3d revealing that zein/HEC crosslinked with PANI/TiO_2 through glutaraldehyde crosslinker.

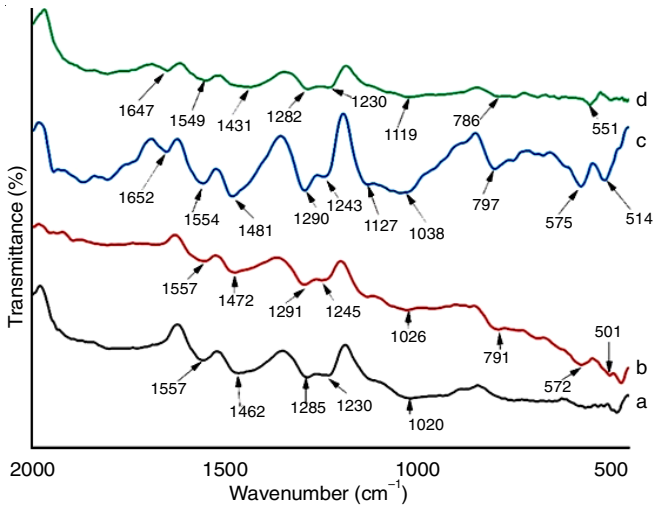

Fig. 3. FTIR spectra of (a) pristine PANI, (b) PANI/TIO_2, (c) zein/HEC/PANI/TiO_2 and (d) glutaraldehyde crosslinked zein/HEC/PANI/TiO_2

Thermal studies: As shown in Fig. 4a, in the decomposition of polyaniline emeraldine salt, two non-linear weight losses were observed from 25 to 100 ºC and from 100 to 310 ºC. The first weight loss was due to the evaporation of water and

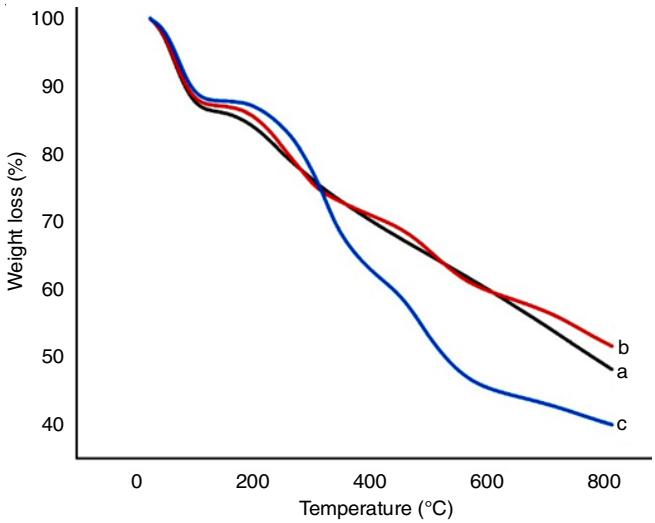

Fig. 4. STA thermograms of (a) pure polyaniline, (b) PANI/TiO_2 and (c) zein/HEC/PANI/TiO_2

a small amount of HCl. In the second case, from 100 to 310 ºC, the primary weight change was due to removal of the dopant (HCl). Additionally, some water molecules firmly attached to the polymer surface were also released [51,52]. Similar to the previous report [50], the weight loss from 300 to 800 ºC showed a linear degradation curve. Most of the molecules removed from 300 to 700 ºC were ammonia and aniline molecules. Above 700 ºC, ammonia and acetylene were the possible degradation products [53].

TiO_2 nanoparticles cannot decompose in the temperature range of 25-800 ºC [54]. Thus, the decomposition of PANI/TiO_2 under this temperature range was due to polyaniline degradation. But, under similar temperature change, the decay of PANI/TiO_2 was less than pure polyaniline as shown in curve 'b'. This proved that thermogravimetric stability of PANI/TiO_2 was higher than pure PANI due to TiO_2 nanoparticle strong interaction with polyaniline [50].

In the thermal degradation of zein/HEC/PANI/TiO_2, three major weight loss changes were observed as shown in (curve c), the first weight change from 25 to 120 ºC was due to the removal of water from the hybrid nanocomposite surface. In the second phase, around 23% weight loss was due to the composite degradation from 220 to 375 ºC temperature ranges [55, 56]. In the third stage, the degradation continued from 390 to 600 ºC due to pyrolysis reactions of HEC [56] and degradation of polyaniline. Above 600 ºC, a linear degradation curve similar to curve 'a' was observed due to further degradation of polyaniline [53]. The weight loss of zein/HEC/PANI/TiO_2 corresponding to 25 to 310 ºC was lower than pure polyaniline and PANI/TiO_2 (curve c), confirmed it's highest thermal stability in this region. The photocatalytic dye degradation reaction favoured between 25 and 80 ºC reaction temperature [57]. Hence, the newly synthesized photocatalyst has better thermal stability for degrading dye molecules.

Photocatalytic activity of Zein/HEC/PANI/TiO_2 composites

Effect of TiO_2 on zein/HEC/PANI/TiO_2 hybrid composite: The hybrid composite catalytic efficiency was evaluated by changing the proportions of TiO_2 nanoparticles under fixed methyl orange concentration, catalyst dosage, pH and reaction time. The degradation efficiency of zein/HEC/PANI/TiO_2 hybrid nanocomposite with TiO_2 proportions of 0, 5, 10, 15 and 20% relative to aniline is shown in Fig. 5. The catalytic reaction efficiency increased with increasing TiO_2 nanoparticles and the highest dye degradation efficiency was achieved at 10% load of TiO_2. Further increasing the nanoparticle decreases catalytic degradation. This is because the catalyst's surface area decreased due to nanoparticles' spontaneous agglomeration at higher proportions of TiO_2 [16]. In addition, a high proportion of TiO_2 prevents the UV light source from striking to polyaniline surface; thus, polyaniline was unable to sensitize the reaction, which leads to decreased degradation [33]. Thus, the amount of TiO_2 nanoparticles in the composite should be lower than polyaniline. Because a high concentration of polyaniline is not only sensitizing the reaction but also effectively stabilizing the nanoparticles of TiO_2 by preventing nanoparticle aggregation [58].

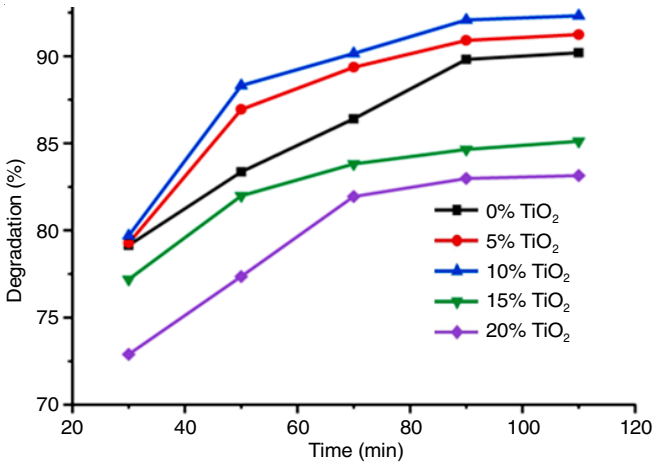

Fig. 5. Effects of TiO_2 proportion on photocatalytic degradation efficiency of zein/HEC/PANI/TiO_2 catalyst

Effect of pH: The catalyst surface and dye solution's charges are affected by the variation of pH in the reaction path. Therefore, it is vital to optimize the pH of the reaction condition to obtain maximum degradation products. Thus, the photocatalytic degradation reaction was performed with different pH values ranging from 2 to 12. The degradation efficiency was decreased when pH goes towards a lower acidic pH less than 4 and higher basic pH more than 10. But in the mild acidic and basic pHs, degradation efficacies were higher as shown in Fig. 6. This is because the zein surface in a mild acidic condition is positively charged due to side amine groups' protonation on glutamine residues [59]. Hence, the anionic methyl orange adsorption on the surface of the catalyst was enhanced, supporting catalytic reaction. But in a strongly acidic solution, it decreased due to the loss of positively charged groups by the change of glutamine into glutamic acid. Similarly, a dramatic decrease in higher basic pH was caused by the generation of negatively charged groups due to deprotonation of carboxylic groups on glutamate. This creates strong electrostatic interaction with anionic dyes, which caused a decrease in the reaction

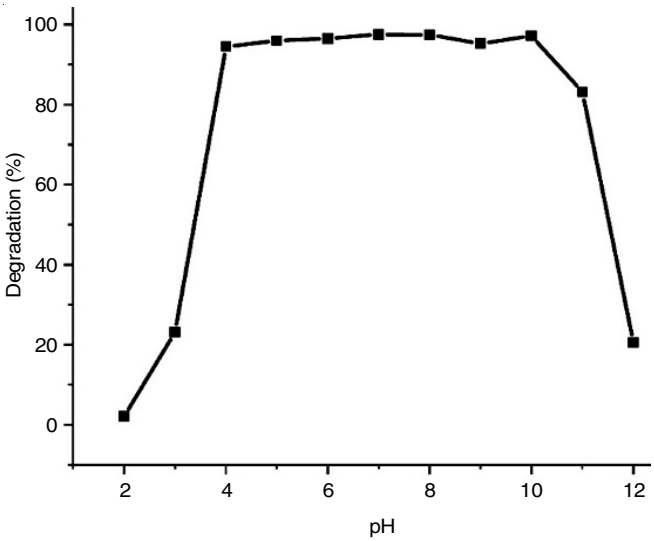

Fig. 6. Effect of pH on photocatalytic degradation of methyl orange by zein/HEC/PANI/TiO_2

[60]. Different amino acid groups were dispersed in a mildly alkaline solution and thus, catalytic degradation was enhanced. Also, PANI/TiO_2 is positively charged in acidic media and negatively charged in higher pH. Hence, the electrostatic force of attraction between the catalyst and dye molecules favoured an acidic environment but diminished in a strong alkaline condition [32]. The neutral and mild alkaline conditions were more efficient than mild acidic conditions as shown in Fig. 6. Sedghi *et al.* [31] also reported similar results using polyaniline modified TiO_2/polyacrylonitrile nanocomposite. With a 95% confidence level, the photocatalytic degradation of methyl orange was strongly affected by acidic (pH < 4) and basic (pH > 10) conditions. However, there were no significant changes in the photocatalytic degradation of methyl orange with the pH ranging from 4 to 10 (Fig. 6). This result depicted that the newly synthesized photocatalyst was efficient in a wide range of pH, which is essential to treat anionic dye wastes without adjusting pH. Even though no substantial change, 97.51% was the maximum degradation efficiency achieved at neutral pH. Hence, it was this pH used for all investigations carried out in this study.

Effect of catalyst dosage: The influence of catalyst dosage on the degradation of methyl orange has been investigated at a pH of 7, 100 mL of 125 µM dye concentration and 110 min degradation time. The quantity of catalysts used was 0.01, 0.02, 0.03, 0.04, 0.05, 0.06, 0.07 and 0.08 g. The efficacy increases with an increasing amount of zein/HEC/PANI/TiO_2 hybrid nanocomposite (Fig. 7). With an increasing amount of catalyst, the number of photons adsorbed on it increased due to the increased number of available active sites. Hence, the number of dye molecules adsorbed on the photoactivated surface increased and thus the rate of degradation is enhanced [61,62]. However, the degradation dependency of dyes with the catalyst higher than 0.03 g was an insignificant increment. When the amount of photocatalyst was beyond the optimum limit, the probability of the dye molecules to bind on the photocatalyst surface becomes equal since there are sufficient active sites.

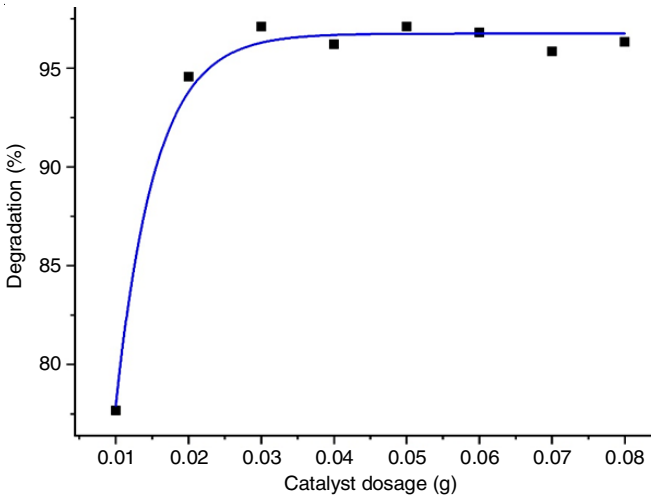

Fig. 7. Effects of zein/HEC/PANI/TiO_2 dosage on the degradation of methyl orange

Thus, the photocatalytic degradation rate becomes nearly constant, whatever the catalyst increased [63].

Efficacy and kinetic study: The photocatalytic activity of zein/HEC/PANI/TiO_2 hybrid nanocomposite was evaluated with and without light. The degradation of methyl orange by zein/HEC/PANI/TiO_2 in the presence of light was considerably higher than in the dark condition as shown in Fig. 8. In dark environment, zein/HEC/PANI/TiO_2 hybrid nanocomposite decolourized about 80.1% dye molecules in 50 min. While more than 91% of dye molecules undergo degradation reaction at the same duration, except the light was irradiated. This confirmed that even though the adsorption is also high, the catalyst degradation efficacy was significantly enhanced with light. The highest removal efficiencies achieved in 110 min with and without light were 97.9% and 84.3%, respectively.

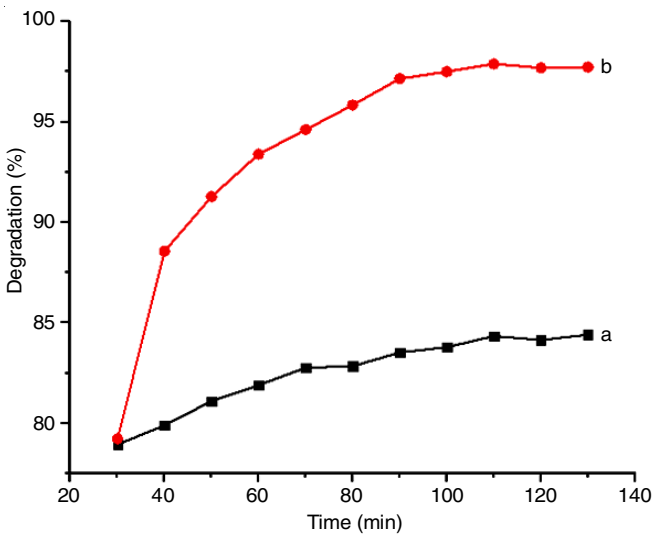

Fig. 8. Degradation of methyl orange by zein/HEC/PANI/TiO_2 (a) without and (b) with light irradiation

The efficiency and overall degradation rate per gram of catalyst and minute of the current investigation were compared with previous reports. As shown in Table-1, zein/HECPANI/

TABLE-1
DEGRADATION EFFICIENCY OF METHYL ORANGE (MO) AND OVERALL RATE COMPARISON WITH PREVIOUS REPORTS

Initial MO concentration (C_o) (mg/L)	Catalyst dose (mg)	Efficiency (%)	Time (adsorption + illumination) (min)	Degradation per g of catalyst (mg/g)	Rate per total time & catalyst (mg/min·g)	Ref.
40.92	30	97.91	110	133.55	1.214	Current study
100.00	10	92	360	920	2.556	[33]
20.00	80	96	360	30	0.083	[43]
10.00	100	100	50	10	0.2	[63]
50.00	100	97.84	120	25	0.208	[64]
3.2733	5	90.3	280	29.62	0.106	[65]
15.00	30	81.4	100	12.21	0.1221	[66]

TiO_2 is the best alternative for degrading a high amount of methyl orange per gram of catalyst in a short duration. The kinetics of the photocatalytic degradation reaction was investigated using the Langmuir-Hinshelwood model. In low concentration, the value $1 + K_2[A]_t$ is nearly equal to unity. The rate law expression becomes a multiple of the apparent rate constant and concentration.

$$\text{Rate} = \frac{-d[A]_t}{dt} = \frac{k_1 K_2 [A]_t}{1 + K_2 [A]_t} \approx K_{app}[A]_t \quad (3)$$

After integration, eqn. 3 can be written as:

$$\ln\left(\frac{[A]_t}{[A]_o}\right) = -k_{app} t \quad (4)$$

where k_1 and K_2 are the reaction rate and the reactant adsorption constants respectively, $[A]_o$ is initial dye concentration, $[A]_t$ is the concentration of the reactant at any time t and K_{app} is the apparent rate constant. From Fig. 9, the correlation coefficient $R^2 = 0.992$ proved that the photocatalytic degradation of methyl orange by zein/HEC/PANI/TiO_2 obeys the kinetics of first order reaction.

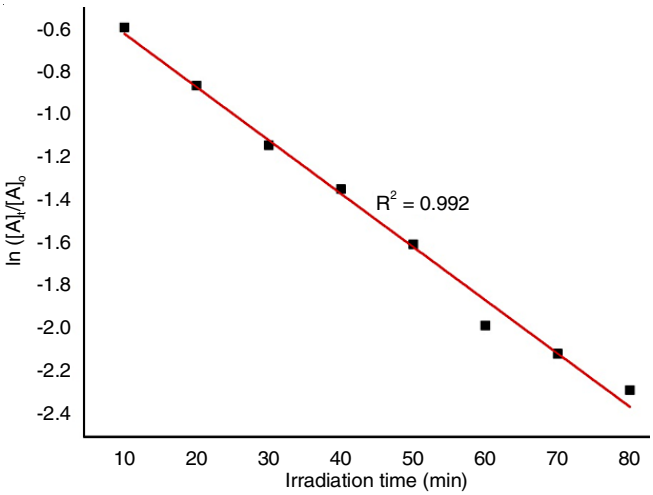

Fig. 9. Kinetic models of first order reaction for methyl orange photocatalytic degradation by zein/HEC/PANI/TiO_2 hybrid nanocomposite

Recyclability evaluation: Recoverability and reusability are essential metrics used to assess the economic viability of the catalyst. Hence, after optimizing TiO_2 proportion, catalyst dose and pH, the catalyst's recoverability was conducted for five cycles. The catalyst's performance corresponding to 1st, 2nd, 3rd, 4th and 5th cycles was 97.91, 96.52, 96.09, 95.14 and 94.03%, respectively. The result indicates that the performance difference between the 1st and the last cycle was small. This shows that glutaraldehyde crosslinked Zein/HEC composite effectively immobilized PANI/TiO_2 photocatalyst. The slight variation between degradation cycles also showed that zein/HEC/PANI/TiO_2 hybrid nanocomposite is a promising photocatalyst in terms of stability and efficacy.

Conclusion

In this investigation, zein/HEC/PANI/TiO_2 hybrid nanocomposite was produced by *in situ* oxidative polymerization followed by immobilization with zein/HEC functionalized composite. The composite of zein/HEC paste effectively immobilized PANI/TiO_2 photocatalyst. More than 97.9% of methyl orange undergoes decolourization within 110 min. Zein/HEC/PANI/TiO_2 photocatalyst performance was 94% after five cycles, indicating its high stability and recyclability. In summary, the newly synthesized photocatalyst is an invaluable alternative for removing dyes (especially anionic dyes) from wastewater.

CONFLICT OF INTEREST

The authors declare that there is no conflict of interests regarding the publication of this article.

REFERENCES

1. P.V. Nidheesh, M. Zhou and M.A. Oturan, *Chemosphere*, **197**, 210 (2018); https://doi.org/10.1016/j.chemosphere.2017.12.195
2. M.M. Hassan and C.M. Carr, *Chemosphere*, **209**, 201 (2018); https://doi.org/10.1016/j.chemosphere.2018.06.043
3. M. Imran, D.E. Crowley, A. Khalid, S. Hussain, M.W. Mumtaz and M. Arshad, *Rev. Environ. Sci. Biotechnol.*, **14**, 73 (2015); https://doi.org/10.1007/s11157-014-9344-4
4. W.S. Wan Ngah, L.C. Teong and M.A.K.M. Hanafiah, *Carbohydr. Polym.*, **83**, 1446 (2011); https://doi.org/10.1016/j.carbpol.2010.11.004
5. D. Mirzaei, A. Zabardasti, Y. Mansourpanah, M. Sadeghi and S. Farhadi, *J. Inorg. Organomet. Polym. Mater.*, **30**, 2067 (2020); https://doi.org/10.1007/s10904-019-01369-9
6. H. Li, S. Liu, J. Zhao and N. Feng, *Colloids Surf. A Physicochem. Eng. Asp.*, **494**, 222 (2016); https://doi.org/10.1016/j.colsurfa.2016.01.048
7. R. Zhang, X. Zhu, Y. Liu, Y. Cai, Q. Han, T. Zhang and Y. Li, *J. Inorg. Organomet. Polym. Mater.*, **29**, 1625 (2019); https://doi.org/10.1007/s10904-019-01125-z
8. S. Khamparia and D.K. Jaspal, *Front. Environ. Sci. Eng.*, **11**, 8 (2017); https://doi.org/10.1007/s11783-017-0899-5
9. M. Rafique, A.J. Shaikh, R. Rasheed, M.B. Tahir, S.S.A. Gillani, A. Usman, M. Imran, A. Zakir, Z.U.H. Khan and F. Rabbani, *J. Inorg. Organomet. Polym. Mater.*, **28**, 2455 (2018); https://doi.org/10.1007/s10904-018-0921-9

10. M. Chen, C. Bao, T. Cun and Q. Huang, *Mater. Res. Bull.*, **95**, 459 (2017); https://doi.org/10.1016/j.materresbull.2017.08.017
11. L.Y. Jun, L.S. Yon, N.M. Mubarak, C.H. Bing, S. Pan, M.K. Danquah, E.C. Abdullah and M. Khalid, *J. Environ. Chem. Eng.*, **7**, 102961 (2019); https://doi.org/10.1016/j.jece.2019.102961
12. M. Jha, S. Ansari and N.G. Shimpi, *J. Ind. Eng. Chem.*, **69**, 269 (2019); https://doi.org/10.1016/j.jiec.2018.09.030
13. S.L. Lee and C. Chang, *Polymers*, **11**, 206 (2019); https://doi.org/10.3390/polym11020206
14. R. Sedghi and F. Heidari, *RSC Adv.*, **6**, 49459 (2016); https://doi.org/10.1039/C6RA02827F
15. R.A. French, A.R. Jacobson, B. Kim, S.L. Isley, L. Penn, P.C. Baveye, *Environ. Sci. Technol.*, **43**, 1354 (2009); https://doi.org/10.1021/es802628n
16. G. Li, L. Lv, H. Fan, J. Ma, Y. Li, Y. Wan and X.S. Zhao, *J. Colloid Interface Sci.*, **348**, 342 (2010); https://doi.org/10.1016/j.jcis.2010.04.045
17. N. Bouazza, M. Ouzzine, M.A. Lillo-Ródenas, D. Eder and A. Linares-Solano, *Appl. Catal. B*, **92**, 377 (2009); https://doi.org/10.1016/j.apcatb.2009.08.017
18. M. Mohsenzadeh, S.A. Mirbagheri and S. Sabbaghi, *Desalination Water Treat.*, **155**, 72 (2019); https://doi.org/10.5004/dwt.2019.23875
19. J. Bhadra, A. Alkareem and N. Al-Thani, *J. Polym. Res.*, **27**, 122 (2020); https://doi.org/10.1007/s10965-020-02052-1
20. H. Zeghioud, N. Khellaf, H. Djelal, A. Amrane and M. Bouhelassa, *Chem. Eng. Commun.*, **203**, 1415 (2016); https://doi.org/10.1080/00986445.2016.1202243
21. M. Hassan, Y. Zhao and B. Xie, *Chem. Eng. J.*, **285**, 264 (2016); https://doi.org/10.1016/j.cej.2015.09.093
22. M. Shah, *J. Appl. Environ. Microbiol.*, **2**, 231 (2014); https://doi.org/10.12691/jaem-2-5-5
23. M. Zhang, Y. Liu, H. Yi, J. Luan, Y. Zhang, H. Cai and D. Sun, *J. Textil. Inst.*, **105**, 246 (2014); https://doi.org/10.1080/00405000.2013.835902
24. F. Liu, R. Li, L. Mao and Y. Gao, *Food Chem.*, **255**, 390 (2018); https://doi.org/10.1016/j.foodchem.2018.02.072
25. N. Ni, D. Zhang and M.J. Dumont, *Polym. Bull.*, **75**, 31 (2018); https://doi.org/10.1007/s00289-017-2017-z
26. H.X. Guo, J. Heinämäki and J. Yliruusi, *J. Colloid Interface Sci.*, **322**, 478 (2008); https://doi.org/10.1016/j.jcis.2007.11.058
27. J.A. Scramin, D. de Britto, L.A. Forato, R. Bernardes-Filho, L.A. Colnago and O.B.G. Assis, *Int. J. Food Sci. Technol.*, **46**, 2145 (2011); https://doi.org/10.1111/j.1365-2621.2011.02729.x
28. W.V.K. Wheelwright, S. Ray and A.J. Easteal, *Mol. Cryst. Liq. Cryst.*, **554**, 252 (2012); https://doi.org/10.1080/15421406.2012.634347
29. M.Y. Rao, K. Harika, K. Sunitha, P.P. Kumar and K. Maheshwar, *Arch. Pharm. Pract.*, **3**, 202 (2012); https://doi.org/10.4103/2045-080X.116598
30. R. Lyu, C. Zhang, T. Xia, S. Chen, Z. Wang, X. Luo, L. Wang, Y. Wang, J. Yu and C.W. Wang, *Colloids Surf. A Physicochem. Eng. Asp.*, **606**, 125425 (2020); https://doi.org/10.1016/j.colsurfa.2020.125425
31. R. Sedghi, H.R. Moazzami, S.S. Hosseiny Davarani, M.R. Nabid and A.R. Keshtkar, *J. Alloys Compd.*, **695**, 1073 (2017); https://doi.org/10.1016/j.jallcom.2016.10.232
32. V.R. Nair and V. Shetty Kodialbail, *Environ. Sci. Pollut. Res. Int.*, **27**, 14441 (2020); https://doi.org/10.1007/s11356-020-07959-2
33. X.F. Song, J.T. Qin, T.T. Li, G. Liu, X.X. Xia, Y.S. Li and Y. Liu, *J. Appl. Polym. Sci.*, **137**, 48516 (2020); https://doi.org/10.1002/app.48516
34. F. Mousli, A. Chaouchi, S. Hocine, A. Lamouri, M. Rei Vilar, A. Kadri and M.M. Chehimi, *Appl. Surf. Sci.*, **465**, 1078 (2019); https://doi.org/10.1016/j.apsusc.2018.09.252
35. S. Razak, M.A. Nawi and K. Haitham, *Appl. Surf. Sci.*, **319**, 90 (2014); https://doi.org/10.1016/j.apsusc.2014.07.049
36. D. Lithner, I. Nordensvan and G. Dave, *Environ. Sci. Pollut. Res. Int.*, **19**, 1763 (2012); https://doi.org/10.1007/s11356-011-0663-5
37. X. Wu, N. Reddy and Y. Yang, *J. Agric. Food Chem.*, **55**, 6279 (2007); https://doi.org/10.1021/jf0633239
38. G. El Fawal, H. Hong, X. Song, J. Wu, M. Sun, C. He, X. Mo, Y. Jiang and H. Wang, *Food Packag. Shelf Life*, **23**, 100462 (2020); https://doi.org/10.1016/j.fpsl.2020.100462
39. J. Yang, L. Zha, D. Yu and J. Liu, *Colloids Surf. B Biointerfaces*, **102**, 737 (2013); https://doi.org/10.1016/j.colsurfb.2012.09.039
40. Z. Liu, Y.-E. Miao, M. Liu, Q. Ding, W.W. Tjiu, X. Cui and T. Liu, *J. Colloid Interface Sci.*, **424**, 49 (2014); https://doi.org/10.1016/j.jcis.2014.03.009
41. N. Singh, P.K. Singh, M. Singh, P. Tandon, S.K. Singh and S. Singh, *J. Mater. Sci. Mater. Electron.*, **30**, 4487 (2019); https://doi.org/10.1007/s10854-019-00737-y
42. M. Liu, Y.E. Miao, C. Zhang, W.W. Tjiu, Z. Yang, H. Peng and T. Liu, *Nanoscale*, **5**, 7312 (2013); https://doi.org/10.1039/c3nr01442h
43. Y. Lin, D. Li, J. Hu, G. Xiao, J. Wang, W. Li and X. Fu, *J. Phys. Chem. C*, **116**, 5764 (2012); https://doi.org/10.1021/jp211222w
44. C. Ratlam, S. Phanichphant and S. Sriwichai, *J. Polym. Res.*, **27**, 183 (2020); https://doi.org/10.1007/s10965-020-02158-6
45. M.J. Antony, C.A. Jolly, K.R. Das and T.S. Swathy, *Colloids Surf. A Physicochem. Eng. Asp.*, **578**, 123627 (2019); https://doi.org/10.1016/j.colsurfa.2019.123627
46. M. Trchová, I. Šedìnková, E. Tobolková and J. Stejskal, *Polym. Degrad. Stab.*, **86**, 179 (2004); https://doi.org/10.1016/j.polymdegradstab.2004.04.011
47. D.M. Jundale, S.T. Navale, G.D. Khuspe, D.S. Dalavi, P.S. Patil and V.B. Patil, *J. Mater. Sci. Mater. Electron.*, **24**, 3526 (2013); https://doi.org/10.1007/s10854-013-1280-5
48. V. Gilja, K. Novakovic, J. Travas-Sejdic, Z. Hrnjak-Murgic, M. Kraljic Rokovic and M. Zic, *Nanomaterials*, **7**, 412 (2017); https://doi.org/10.3390/nano7120412
49. M. Tanzifi, M.T. Yaraki, M. Karami, S. Karimi, A.D. Kiadehi, K. Karimipour and S. Wang, *J. Colloid Interface Sci.*, **519**, 154 (2018); https://doi.org/10.1016/j.jcis.2018.02.059
50. M.R. Karim, H.W. Lee, I.W. Cheong, S.M. Park, W. Oh and J.H. Yeum, *Polym. Compos.*, **31**, 83 (2010); https://doi.org/10.1002/pc.20769
51. M. Dinari and S. Neamati, *Colloids Surf. A Physicochem. Eng. Asp.*, **589**, 124438 (2020); https://doi.org/10.1016/j.colsurfa.2020.124438
52. Y. Wei and K.F. Hsueh, *J. Polym. Sci. A Polym. Chem.*, **27**, 4351 (1989); https://doi.org/10.1002/pola.1989.080271312
53. M.K. Traore, W.T.K. Stevenson, B.J. McCormick, R.C. Dorey, S. Wen and D. Meyers, *Synth. Met.*, **40**, 137 (1991); https://doi.org/10.1016/0379-6779(91)91770-B
54. X. Li, W. Chen, C. Bian, J. He, N. Xu and G. Xue, *Appl. Surf. Sci.*, **217**, 16 (2003); https://doi.org/10.1016/S0169-4332(03)00565-8
55. G.W. Selling, *Polym. Degrad. Stab.*, **95**, 2241 (2010); https://doi.org/10.1016/j.polymdegradstab.2010.09.013
56. R. Chen, C. Yi, H. Wu and S. Guo, *Carbohydr. Polym.*, **81**, 188 (2010); https://doi.org/10.1016/j.carbpol.2010.02.012
57. A. Kumar, *Mater. Sci. Eng. Int. J.*, **1**, 106 (2017); https://doi.org/10.15406/mseij.2017.01.00018
58. M.V. Carevic, N.D. Abazovic, M.N. Mitric, G. Ciric-Marjanovic, M.D. Mojovic, S.P. Ahrenkiel and M.I. Èomor, *Mater. Chem. Phys.*, **205**, 130 (2018); https://doi.org/10.1016/j.matchemphys.2017.11.016
59. Y. Jiao, X. Zheng, Y. Chang, D. Li, X. Sun and X. Liu, *Food Funct.*, **9**, 117 (2018); https://doi.org/10.1039/C7FO01652B
60. B. Zhang, Y. Luo and Q. Wang, *Food Chem.*, **124**, 210 (2011); https://doi.org/10.1016/j.foodchem.2010.06.019
61. K. Pandiselvi and S. Thambidurai, *J. Desalin Water Treat.*, **57**, 8343 (2016); https://doi.org/10.1080/19443994.2015.1019365
62. V. Eskizeybek, F. Sari, H. Gülce, A. Gülce and A. Avci, *Appl. Catal. B*, **119-120**, 197 (2012); https://doi.org/10.1016/j.apcatb.2012.02.034
63. Y. Li, H. Zhao and M. Yang, *J. Colloid Interface Sci.*, **508**, 500 (2017); https://doi.org/10.1016/j.jcis.2017.08.076
64. H. Qi, H. Liu, L. Zhang and J. Wu, *J. Inorg. Organomet. Polym. Mater.*, **29**, 564 (2019); https://doi.org/10.1007/s10904-018-1031-4
65. A.P. Shah, S. Jain, V.J. Mokale and N.G. Shimpi, *J. Ind. Eng. Chem.*, **77**, 154 (2019); https://doi.org/10.1016/j.jiec.2019.04.030
66. K. Yao, Y. Liu, H. Yang, J. Yuan and S. Shan, *Colloids Surf. A Physicochem. Eng. Asp.*, **603**, 125240 (2020); https://doi.org/10.1016/j.colsurfa.2020.125240